BRAIN
ORIGINAL ARTICLE

Magnetic resonance reveals mitochondrial dysfunction and muscle remodelling in spinal muscular atrophy

Laura E. Habets,[1] Bart Bartels,[1] Fay-Lynn Asselman,[2] Melissa T. Hooijmans,[3] Sandra van den Berg,[3] Aart J. Nederveen,[3] W. Ludo van der Pol[2,†] and Jeroen A. L. Jeneson[1,†]

[†]These authors contributed equally to this work.

Genetic therapy has changed the prognosis of hereditary proximal spinal muscular atrophy, although treatment efficacy has been variable. There is a clear need for deeper understanding of underlying causes of muscle weakness and exercise intolerance in patients with this disease to further optimize treatment strategies. Animal models suggest that in addition to motor neuron and associated musculature degeneration, intrinsic abnormalities of muscle itself including mitochondrial dysfunction contribute to the disease aetiology.

To test this hypothesis in patients, we conducted the first *in vivo* clinical investigation of muscle bioenergetics. We recruited 15 patients and 15 healthy age and gender-matched control subjects in this cross-sectional clinico-radiological study. MRI and ^{31}P magnetic resonance spectroscopy, the modality of choice to interrogate muscle energetics and phenotypic fibre-type makeup, was performed of the proximal arm musculature in combination with fatiguing arm-cycling exercise and blood lactate testing. We derived bioenergetic parameter estimates including: blood lactate, intramuscular pH and inorganic phosphate accumulation during exercise, and muscle dynamic recovery constants. A linear correlation was used to test for associations between muscle morphological and bioenergetic parameters and clinico-functional measures of muscle weakness.

MRI showed significant atrophy of triceps but not biceps muscles in patients. Maximal voluntary contraction force normalized to muscle cross-sectional area for both arm muscles was 1.4-fold lower in patients than in controls, indicating altered intrinsic muscle properties other than atrophy contributed to muscle weakness in this cohort. *In vivo* ^{31}P magnetic resonance spectroscopy identified white-to-red remodelling of residual proximal arm musculature in patients on the basis of altered intramuscular inorganic phosphate accumulation during arm-cycling in red versus white and intermediate myofibres. Blood lactate rise during arm-cycling was blunted in patients and correlated with muscle weakness and phenotypic muscle makeup. Post-exercise metabolic recovery was slower in residual intramuscular white myofibres in patients demonstrating mitochondrial ATP synthetic dysfunction in this particular fibre type.

This study provides the first *in vivo* evidence in patients that degeneration of motor neurons and associated musculature causing atrophy and muscle weakness in 5q spinal muscular atrophy type 3 and 4 is aggravated by disproportionate depletion of myofibres that contract fastest and strongest. Our finding of decreased mitochondrial ATP synthetic function selectively in residual white myofibres provides both a possible clue to understanding the apparent vulnerability of this particular fibre type in 5q spinal muscular atrophy types 3 and 4 as well as a new biomarker and target for therapy.

1   Centre for Child Development, Exercise and Physical Literacy, Wilhelmina Children's Hospital, University Medical Centre Utrecht, P.O. Box 85090, 3508 AB Utrecht, The Netherlands
2   UMC Utrecht Brain Centre, Department of Neurology and Neurosurgery, University Medical Centre Utrecht Brain Center, Utrecht University, P.O. Box 85500, 3508 GA Utrecht, The Netherlands
3   Department of Radiology & Nuclear Medicine, Amsterdam Movement Sciences, Amsterdam University Medical Centre, Location AMC, 1105 AZ Amsterdam, The Netherlands

Correspondence to: J. A. L. Jeneson
Centre for Child Development, Exercise and Physical Literacy, Wilhelmina Children's Hospital
University Medical Centre Utrecht, KB 02.056.0, PO Box 85090, 3508 GA Utrecht, The Netherlands
E-mail: j.a.l.jeneson@umcg.nl

Introduction

5q Spinal muscular atrophy (5qSMA) is an important genetic cause of infant mortality, severe and progressive physical disability in children and adults and is caused by homozygous loss of function of the *survival motor neuron 1* gene.[1] Deficiency of the ubiquitously expressed survival motor neuron protein interferes with a range of basic cellular processes, including splicing and ribosomal translation of mRNA.[2] In α-motor neurons survival motor neuron protein deficiency is associated with progressive destabilization of axonal end-plates and ultimately denervation and atrophy of associated skeletal musculature.[3]

Large and fast-conducting motor neurons and their associated pools of fast-twitch glycolytic 'white' myofibres appear to be particularly vulnerable to neuronal survival motor neuron protein deficiency.[4,5] This hypothesis is supported by the prevalence of the most prominent symptom in 5qSMA, muscle weakness,[6,7] as well as by *ex vivo* and *in vitro* examinations of muscle biopsy samples from patients with 5qSMA and SMA mouse models,[8–10] respectively. Abnormal muscular fatigability is, however, also common in 5qSMA.[11–14] Since fatigue resistance of any muscle scales with contractile energetic efficiency and ATP synthetic capacity,[15] this particular symptom suggests that the functionality of motor units comprising oxidative myofibre phenotypes (i.e. slow-twitch oxidative 'red' and fast-twitch oxidative glycolytic 'intermediate' myofibres, respectively)[4,5,16] is also affected in 5qSMA. Indeed, there is evidence that intrinsic abnormalities in muscle itself may contribute to the disease phenotype.[17,18] For example, several studies of SMA have found mitochondrial abnormalities in animal models and muscle *ex vivo* that may cause energetic failure of excitation–contraction coupling preservation during muscular work.[15,18–23] Moreover, results of a recent investigation in an SMA mouse model indicate that mitochondrial ATP synthetic capacity is dysfunctional specifically in white myofibres.[22] Any mechanistic link between survival motor neuron protein depletion and abnormal muscular phenotypic traits in 5qSMA is yet to be identified.[17,18]

Various studies have used MRI to investigate muscle morphology in 5qSMA.[24–27] *In vivo* ^{31}P magnetic resonance spectroscopy (^{31}P MRS) is a complementary, non-invasive method to additionally study metabolic phenotypic traits of muscle including *in vivo* mitochondrial function.[16] Of particular interest to 5qSMA, integration of ^{31}P MRS with in-magnet voluntary exercise paradigms can capture and distinguish metabolic manifestations of functional innervation of intramuscular pool of red, intermediate and white

myofibres, respectively, in a muscle.[28,29] Here, we apply the power of these *in vivo* methodologies to study muscle morphology and metabolic phenotypic traits in relation to function in adolescent and adult patients with 5qSMA types 3 and 4. Our work provides *in vivo* evidence that both neurogenic as well as intrinsic muscular abnormalities contribute to the clinical phenotype of the disease.

Materials and methods

Participants

We recruited patients with 5qSMA types 3a, 3b and 4 registered in the Dutch SMA registry for this study. All patients had a confirmed homozygous deletion of the SMN1 gene. We used the clinical classification system based upon age of onset and acquired motor milestones to distinguish between 5qSMA types 2–4.[30] In case of discrepancies between age at symptom onset and highest achieved motor milestones, the latter determined classification. Patients with 5qSMA type 3a, 3b and 4 show clinical symptoms before the age of three, after the age of 3 and during adult life, respectively. Age and gender-matched control participants were recruited with the help of the patient's social network of family and friends and via social media. Inclusion criteria were: (i) age ⩾12; (ii) ability to perform active supine arm-cycling movements; (iii) ability to follow test instructions; and (iv) musculus biceps brachii (BB) Medical Research Council score for muscle strength ⩾4 and musculus triceps brachii (TB) Medical Research Council score ⩾2. Exclusion criteria were: (i) contraindications concerning magnetic resonance assessment; (ii) risk factors for exercise testing registered by a Dutch version of the Preparticipation Questionnaire (American College of Sports Medicine and American Heart Association); (iii) mental retardation; (iv) comorbidities affecting exercise tolerance; and (v) being under examination for non-diagnosed disease at the time of investigation. The Medical Ethics Committee of the University Medical Centre Utrecht in the Netherlands approved the study (NL62792.041.17). All participants (and their parents) signed appropriate informed consent.

Study design

This cross-sectional clinical investigation consisted of two visits separated by at least 1 week to minimize the influence of exercise induced fatigue (Fig. 1A). The first visit took place at the Centre for Child Development, Exercise and Physical Literacy at the
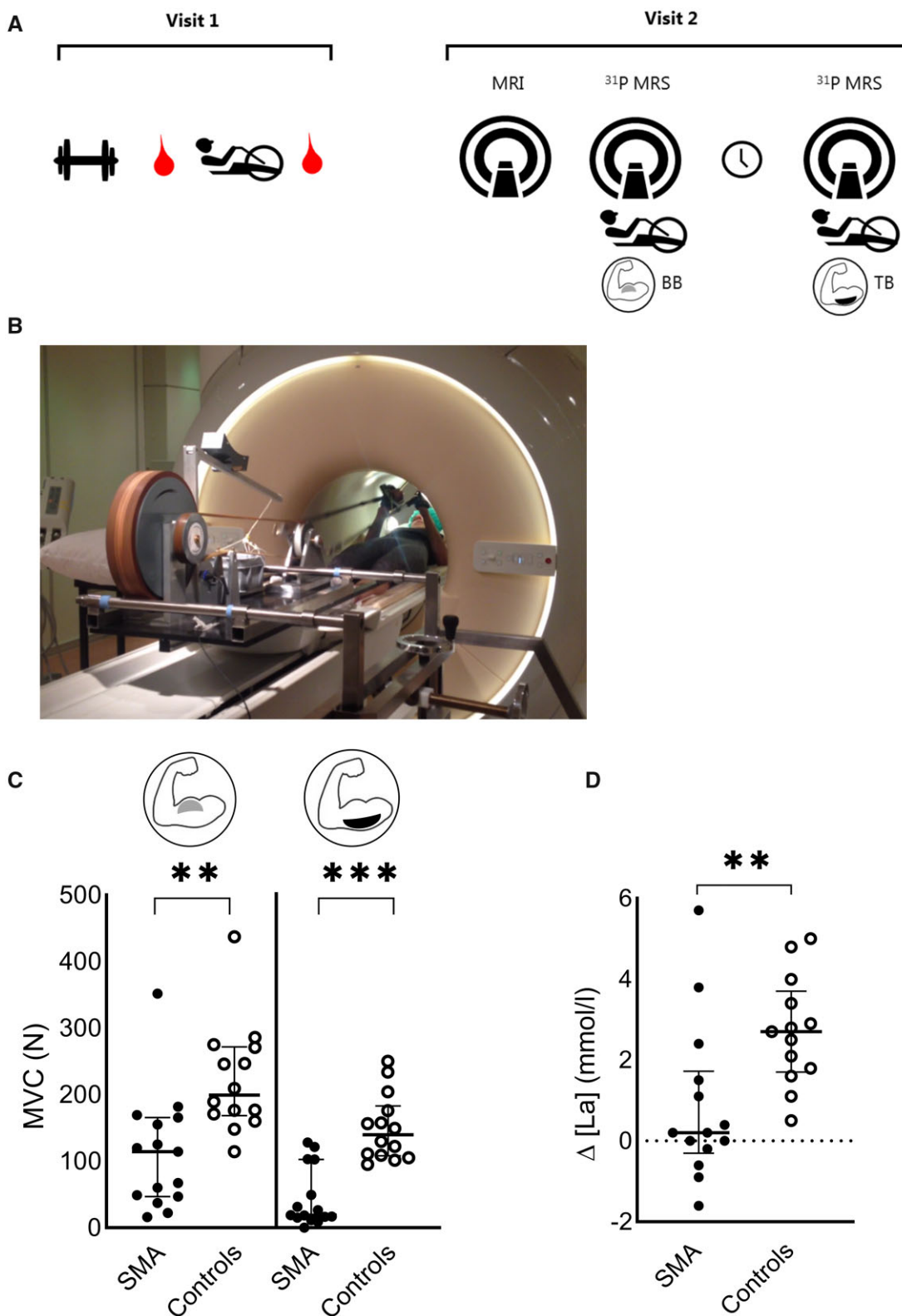
Figure 1 Experimental design and first visit results. (**A**) Study design. (**B**) The experimental set-up used for supine arm-cycling inside the bore of a 3 T multinuclear MRI scanner (Ingenia scanner with 70 cm bore diameter, Philips Healthcare). (**C**) Median, interquartile range (IQR) and individual maximal voluntary contraction (MVC) force (N) of patients with 5qSMA and controls measured in the BB (P = 0.002) and TB (P < 0.001) muscle. (**D**) Median, IQR and individual Δ capillary blood lactate (La) (mmol/l) measured in patients with 5qSMA and controls (P = 0.004). **P < 0.01, ***P < 0.001.

University Medical Centre Utrecht, The Netherlands. First, participants performed maximal voluntary contractions measured with a handheld dynamometer using the break test (MicroFET2, Hoggan Health Industries), as described elsewhere.[31] Thereafter, a supine arm-cycling test outside the magnetic resonance scanner was performed. We measured capillary blood lactate, caught in lithium

heparin micro cups (Greiner Bio-One B.V., catalogue number 450550) before and directly after cycling using a finger stick. Lactate is a metabolic product of anaerobic glycolysis and is rapidly exchanged with the extracellular milieu.[32] As such, any increase in blood lactate during exercise is generally viewed on metabolic activity of white myofibres in active muscles.[33] The second visit took place at the Amsterdam University Medical Centre, location AMC. After an MRI of the upper arm, participants were asked to perform an incremental supine arm-cycling test twice at the same day. A resting period of 20–30 min separated the two sessions of exercise.

Supine arm-cycling test

A previously described magnetic resonance-compatible mechanically braked bicycle ergometer adjusted for asynchronous arm-cycling with two length-adjustable carbon ski poles (Leki) with custom made 3D printed carbon handles was used for physical exercise of the upper arm muscles (Fig. 1B).[34,35] Pole handles were additionally fitted with adjustable gloves from cross-country ski poles (Leki, Italy) to minimize involvement of muscles of the forearm during execution of the cycling task (Supplementary Fig. 9). Last, the platform was fitted with a mounting system for the mobile Lode magnetic resonance ergometer carrier (Lode) allowing flexible positioning over the patient bed of the magnetic resonance scanner (Fig. 1B). The supine arm-cycling test was performed with an angle of 90° elbow flexion at the neutral starting position of vertical cranks. After 5 min of rest, participants were asked to cycle until exhaustion to ensure myofibre recruitment across the spectrum according to Henneman's size principle.[36] Lower arms moved between –45° and + 45° in the z-direction at 90 rpm.

The rate of 90 rpm was indicated by an audio cue. Two patients with 5qSMA cycled on a rate of 45 rpm. The test started with 6 min of cycling at 5 W on the magnetic resonance-compatible ergometer. Subsequently, a mechanical brake aggravated the protocol to 10 W for 1 min. A weight of 0.2 kg for female and 0.3 kg for male participants was added to increase the resistance every minute thereafter. Post-exercise recovery was monitored for 10 to 20 min. The BB was measured during the first, and the TB during the second cycling test at the second visit (Fig. 1A). We measured acceptability of the study visits and perceived fatigue in participants on a visual analogue scale and OMNI scale of perceived exertion on a range between 0 and 10, respectively.

MRI

MRI data acquisition

MRIs were obtained to provide insight in upper arm muscle morphology of patients with 5qSMA and controls. All magnetic resonance experiments were conducted on the 70 cm wide-bore diameter 3 T Ingenia multinuclear MR system (Philips Healthcare). Participants were positioned on their right side and head first into the scanner. Neck, back and legs were supported based on individual preferences. Sand bags fixated the right upper and lower arm, which was positioned to the centre of the bench as much as possible. Datasets were acquired from the right upper arm using a 16-channel Anterior Receive coil positioned on the torso of the participant covering the whole arm and 12-channel coil located in the patient table. The imaging protocol consisted of survey scans used for accurate placement of the Dixon sequence and a 4-point Dixon sequence (TR/TE/ΔTE 210/2.6/0.76 ms; flip angle 8°; field-of-view $480 \times 276 \times 198$ mm; acquisition voxel size $1.5 \times 1.5 \times 6$ mm^2; reconstruction voxel size $1.5 \times 1.5 \times 6$ mm; no gap; number of slices 33; SENSE 2) for fat quantification and muscle volume assessments.[37]

MRI data analysis

MRIs were analysed using QMRITools for Mathematica (https://mfroeling.github.io/QMRITools, accessed 22 February 2022). Dixon data were processed using iterative decomposition of water and fat with echo asymmetry and least squares estimation (IDEAL) using eight reference fat peaks and considering a single T_2^* decay. Muscle morphology was described by fat percentage and contractile cross-sectional area of the muscle. Fat fractions were calculated as the signal intensity (SI) fat/(SI fat + SI water) $\times$ 100 and contractile cross-sectional area was calculated by the following equation: contractile cross-sectional area = CSA $\times$ (100 – %fat). Regions of interest for the BB and TB were manually drawn on the reconstructed water image of the Dixon scan using ITK-SNAP (www.itksnap.org, accessed 22 February 2022)[38] on the slice with the largest CSA. First, the largest CSA was determined for each muscle individually using visual assessment. After which regions of interest were drawn on those slices, specifically and used to derive the CSA, percentage of fat and the contractile cross-sectional area of BB and TB separately.

Muscle ^{31}P magnetic resonance spectroscopy
Magnetic resonance spectroscopy data acquisition

A 6 cm diameter single turn ^{31}P surface coil (Rapid Biomedical) was fastened over either the BB or TB, respectively, of the right upper arm. Head and knees were supported on individual preferences. Upper arms were stabilized with a cushion to prevent movement during the preparation phase of MRS data acquisition. Participants were moved into the magnet centre and a scout image was acquired to direct shimming. ^{31}P magnetic resonance spectra from upper arm muscles were collected at rest, during arm-cycling and subsequent metabolic recovery (block pulse, flip angle 45°; TR: 4000 ms; NSA 2; 2048 data-points; bandwidth 3000 Hz). The bottom bracket of the platform approached the bore no more than 50 cm to prevent influence of the magnetic field on the cycling resistance. Data acquisition during arm-cycling was synchronized with the cycling rate as described elsewhere.[35]

Magnetic resonance spectroscopy data analysis

Datasets were analysed blindly by one observer (J.A.L.J.). FIDs were analysed using AMARES time domain fitting (www.jMRUI.org) with customized starting value and prior knowledge files. Myofibre pH was derived from the chemical shift difference between the inorganic phosphate (Pi) and phosphocreatine (PCr) resonances.[35] Myofibre phenotypes were attributed by (i) phenotypic fingerprint at end state of exercise; and (ii) by PCr and Pi 95% recovery times. Phenotypic fingerprint, expressed in the fraction of Pi signals from recruited myofibres, was examined in participants showing a PCr depletion of >90% at the point of exhaustion. We included two patients with a PCr depletion between 80 and 90% and we excluded one patient with a PCr depletion <80%. The latter showed decrement (>10%) of the m. trapezius during repetitive nerve stimulation of the n. accessorius. Post-exercise metabolic recovery kinetics (Fig. 4C and D) were determined by nonlinear curve fitting of mono- or double-exponential functions.[39] Pi and PCr 95% recovery times in minutes were calculated by the following equation: 0.95 $\times$ [3 $\times$ tau(min)].

Statistical analysis

We used two tailed parametric t-tests to examine differences in contractile cross-sectional area and PCr 95% recovery times between patients with 5qSMA and healthy controls. We used non-parametric Mann–Whitney U-tests to examine differences in

maximal voluntary contractions, Δ capillary blood lactate, fat infiltration, phenotypic fingerprint and Pi$_{(red, intermediate, white)}$ 95% recovery time between patients with 5qSMA and healthy controls. An allometric function was used to fit associations between MRI parameters. We used Pearson's correlations to assess the relationship between maximal voluntary contraction force and contractile cross-sectional area of both muscles. We used Spearman's correlations to assess the relationship between maximal voluntary contraction force and Δcapillary blood lactate, Δcapillary blood lactate and Pi$_{IM + White}$. The level of significance was set at $P < 0.05$.

Data availability

The data that support the findings of this study are available from the corresponding author (J.A.L.J.) on reasonable request.

Results

Experimental paradigm to assess upper arm muscle

To probe the relation between function and muscle quality and quantity, our experimental design featured functional testing (maximal voluntary contraction and dynamic voluntary exercise), morphological (^{1}H MRI) and metabolic studies (blood sampling and *in vivo* ^{31}P MRS) in a cohort of treatment naïve patients with genetically confirmed 5qSMA (Fig. 1A; 'Materials and methods' section). To overcome the communal practical problem of proximal muscle weakness and lower body disability in this patient group, we switched from a leg-cycling to an arm-cycling exercise platform (Fig. 1B and Supplementary Video 1).[40,41] We recruited a total of 15 patients with 5qSMA and 15 age- and gender-matched healthy controls (Table 1 and Supplementary Table 1). Of our 15 patients with 5qSMA, six were classified as 5qSMA type 3a (four non-ambulant patients; Supplementary Table 1, Cases 4, 6, 11 and 15), eight as type 3b and one as type 4. Patient acceptability of the magnetic resonance exercise intervention, measured on a visual analogue scale ranging from 0 to 10 indicating willingness to repeat this test in any future clinical study, was excellent in patients [mean (SD): 9.1 (1.3)] and controls [8.3 (2.3)]. One control participant dropped out after the first visit.

Maximal voluntary contraction (MVC) force of BB and TB muscles in patients was significantly lower compared to controls reflecting muscle weakness, the hallmark symptom of 5qSMA (Fig. 1C); $P = 0.002$, $P < 0.001$, respectively. Blood lactate increase in response to arm-cycling exercise was significantly lower in patients compared to controls (Fig. 1D) ($P = 0.004$) and uncorrelated to cycling time in the large majority of patients (Supplementary Fig. 1). Cycling time between bouts in the second visit was highly reproducible in both groups, but significantly shorter in patients compared to controls {BB [mean (SD)]: 3.1 (1.9), TB: 3.0 (2.1) min. versus BB: 7.4 (1.3), TB: 7.2 (2.4) min., respectively; $P < 0.001$]} recapitulating previous observations of exercise intolerance and premature fatigability in 5qSMA.[13] Perceived fatigue was similar in patients compared to controls {BB [median (IQR)]: 9.0 (2.0), TB: 9.0 (4.0) versus BB: 9.0 (5.0),TB: 9.0 (7.0), respectively; $P > 0.05$)}.

Morphology of upper arm muscles in adolescent and adult 5qSMA

We acquired magnetic resonance images of the upper arm to examine fat infiltration and atrophy of the BB and TB muscles of the right arm of patients with 5qSMA ($n = 13$) and controls ($n = 14$) using a four-point Dixon sequence. Two patients with 5qSMA had contraindications concerning MRI assessment. A set of typical transverse images of the upper arm of a patient versus a healthy

control are shown in Fig. 2A, with BB and TB indicated in red. Visual inspection of the images indicated that fat infiltration and loss of muscle mass as previously reported for leg muscles in patients with 5qSMA were also present in the upper arm muscles of patients.[24] To objectify this trend, we performed quantitative image analyses using QMRITools for Mathematica (Materials and methods) and found that fat percentages of both BB as well as TB were significantly higher in patients than controls (Fig. 2B); $P = 0.007$, $P < 0.001$, respectively. Our findings mirror the 11.9–15.5% fatty infiltration in the BB muscle of patients with 5qSMA type 3 reported previously.[25] On the other hand we found a higher fat percentage in the TB muscle of patients in our cohort than the previously reported 12.9–20.3%.[25] Contractile cross-sectional area of the TB muscle, defined as gross CSA adjusted for fatty infiltration, was significantly reduced in patients compared to controls (Fig. 2C); $P < 0.001$. BB contractile cross-sectional area was not different in patients and controls (Fig. 2C) ($P = 0.309$) suggesting this muscle of the upper arm was more preserved than its antagonist in this particular cohort. Fat infiltration negatively correlated with the contractile cross-sectional area for both BB and TB ($r = –0.71$ and –0.80, $P < 0.0001$, respectively; Fig. 2D and E).

Metabolic phenotypic profiling of upper arm muscles in adolescent and adult 5qSMA

Integration of ^{31}P MRS with in-magnet voluntary exercise models for human lower limb muscles has been shown to capture and distinguish metabolic manifestations of working red, intermediate and white myofibre pools, respectively.[28,29] To test whether this methodology can be used to evaluate residual functional innervation of each of these fibre-type pools in the upper arm muscles of patients with 5qSMA, we first performed dynamic recording of *in vivo* ^{31}P magnetic resonance spectra from the BB muscle in a healthy subject performing the arm-cycling trial. We observed multiple distinct peaks between 5.2 and 3.7 ppm in *in vivo* ^{31}P magnetic resonance spectra from this working muscle (Fig. 3A) that exhibited extraordinary temporal dynamics as exercise continued until exhaustion (Supplementary Fig. 2). A point of note is that these spectral dynamics presented early into exercise in the presence of high total muscle content of the myofibrillar ATP buffer PCr (0.0 ppm). Previous studies in human lower limb muscles reported such observations only late into exercise in the presence of large PCr depletion.[28,39,42] Similar observations were made in the TB muscle (Supplementary Fig. 3). On the basis of previous work, we attributed the detected ^{31}P magnetic resonances between 5.2 and 3.7 ppm to Pi, a metabolic product of ATP hydrolysis, accumulating in red, intermediate and white myofibres operating at distinct cytoplasmic pH values ranging between pH 7 and 6 (Fig. 3A and B and Supplementary Fig. 4).[28,39,42]

We next hypothesized that the observed rich Pi and pH dynamics in working BB and TB muscles captured motor unit recruitment in action on the premise that arm-cycling represents an uncommon motor task in daily life and has been associated with short-term motor skill learning in naïve subjects.[34,43] As such, once all available motor units have been recruited, the particular *in vivo* ^{31}P magnetic resonance spectral BB and TB fingerprint at that time should inform on the relative abundance of red, intermediate and white myofibre pools with functional innervation in these muscles. We then estimated these fractions for each myofibre type on the basis of numerically fitted fractional amplitudes of Pi resonances at 5 ppm (pH 7, red fibres), 4.6–4.2 ppm (pH 6.6 ± 0.1, intermediate fibres) and 4 ppm (pH 6, white fibres), respectively (see 'Materials and methods' section; Supplementary Fig. 5) as described previously.[39] Assuming the condition of complete motor unit recruitment is adequately satisfied when total muscle PCr is

Table 1 Cohort demographic characteristics

Demographic	Age, years	Percentage male	5qSMA type 3a/ 3b/4 (n)	SMN copy no. 3/ 4 (n)	HFMSE	MRC score BB (range)	MRC score TB (range)
Controls (n = 14)	40 ± 17	36	n.a.	n.a.	n.a.	5	5
5qSMA (n = 15)	40 ± 17	33	6/8/1	3/12	40 ± 18	4–5	3–5

Values are expressed as mean ± SD, subtype 3a clinical symptoms <3 years, subtype 3b clinical symptoms >3 years. HFMSE = Hammersmith Functional Motor Scale Expanded; MRC = Medical Research Council score for muscle strength; n.a. = not applicable.

90% or more depleted,[42,44] we verified in a healthy subject that analysis of the ^{31}P magnetic resonance spectrum of the BB muscle at fatigue recorded in two separate arm-cycling trials yielded reproducible estimates of its functional phenotypic myofibre makeup in this individual (Supplementary Table 2). The resulting outcome of a predominantly fast-twitch white myofibre phenotype is in good agreement with histological studies of the BB muscle of healthy adults.[45–47]

We next collected *in vivo* ^{31}P magnetic resonance spectra of the BB and TB muscles during exhaustive arm-cycling in patients (n = 15) and controls (n = 14) to compare the relative abundance of red, intermediate and white myofibres with functional innervation, respectively, in these muscles. Time to PCr depletion was 4- to 8-fold shorter in 5qSMA than in controls [BB: 64 s, 32–92 versus 288 s, 144–328 (median, IQR), P = 0.055, respectively, TB: 48, 28–128; 320, 120–352, P = 0.029]. Comparison of the group medians of the fractional size of functional red versus intermediate and white myofibre pools in the BB and TB muscles in 5qSMA versus controls (Fig. 3C and D) identified a trend towards a white-to-red shift in functional myofibre makeup for the TB muscle of patients compared to controls (Fig. 3D; P = 0.101). This white-to-red shift was significant for the BB muscle of patients (Fig. 3C; P = 0.0045).

In vivo mitochondrial function in arm muscle in adolescent and adult 5qSMA

Restoration of the resting energetic state of myofibres following muscular work is principally driven by mitochondrial ATP synthesis.[44,48] Therefore, we continued recording *in vivo* ^{31}P magnetic resonance spectra from BB and TB muscles after arm-cycling had stopped to test our hypothesis that this ATP synthesis in muscle is compromised in 5qSMA.[19,20] We found that full recovery of PCr and Pi levels to pre-exercise concentrations may take up to 10 min in patients with 5qSMA (Fig. 4A and B) and that the divergence in myoplasmic pH between red, intermediate and white fibre types developed during the preceding exercise, persisted during all this time (Supplementary Fig. 6). This uniquely afforded tracking and quantification of Pi recovery times for each myofibre phenotype (Fig. 4C) in addition to the standard approach of tracking total muscular PCr content (Fig. 4D).[16]

In the control group, mean 95% recovery time for Pi in red and intermediate fibre types was the same within each muscle (Fig. 4C) but significantly faster in BB muscle compared to TB (Fig. 4C; P = 0.013). Median Pi 95% recovery time for white myofibres in this group was 5-fold slower (Fig. 4C) compared to red myofibres and similar in both muscles. This 1:1:5 ratio for Pi 95% recovery time in human red, intermediate and white myofibre phenotypes, respectively, mirrors the ratio of *in vivo* initial rates of post-exercise Pi recovery in these fibre types reported previously for leg muscle of healthy individuals.[42] This outcome fits well with findings of 5-fold lower measures of mitochondrial density and 6-fold fewer embedded capillaries for white compared to red myofibres,[49,50] respectively, in rodent muscles. Likewise, mean 95% recovery time for total PCr in BB and TB muscles (Fig. 4D) matched previous reports of PCr recovery times following strenuous exercise.[51,52]

In the patient group, median Pi 95% RTs for red and intermediate myofibres of BB and TB muscles were identical to controls (Fig. 4C). In contrast, median 95% recovery time for Pi in white myofibres of BB muscles was almost 2-fold longer than in controls (Fig. 4C); P = 0.031. Pi recovery in white myofibres of the TB muscle of patients was similarly prolonged in two of four available datasets from this group (Fig. 4C). These results indicate that mitochondrial ATP synthetic function is compromised in white, but not red or intermediate myofibres of arm muscle in the patient group. Our findings that post-exercise recovery of total muscular PCr in patients was either not prolonged (BB muscle; P = 0.764) or even faster (TB muscle; P = 0.025) compared to controls (Fig. 4D) both fit this conclusion and confirm white-to-red muscle remodelling in the patient group.

Relationship between muscle ultrastructure, phenotypic traits and function in 5qSMA

Our study has revealed associations between function (Fig. 1C), morphological (Fig. 2) and metabolic phenotypic traits (Figs 3 and 4) of upper arm musculature in 5qSMA. Next, we investigated whether it was possible for each of these traits to predict residual function of these muscles in patients. First, we tested the hypothesis that muscles with a larger functional mass generate more power. Indeed, we found strong positive correlations between MVC force and contractile cross-sectional area for both the BB and TB muscles in patients with 5qSMA and controls [r = 0.89, 95%CI: 0.77–0.95 and r_s (130) = 0.96, respectively, P < 0.001; Fig. 5A and B]. Combining these functional and morphological datasets we compared force per contractile cross-sectional area between patients and controls. For both the BB and TB muscles this parameter was 1.4-fold reduced in the patient group (P < 0.01 for BB; Supplementary Fig. 7). Next, we proposed that the reduced power of the BB and TB muscles of patients was associated with a lower abundance of white and intermediate myofibres with functional innervation compared to controls (Fig. 4C and D). We then tested a first corollary that any increase in capillary blood lactate in response to arm-cycling would be blunted in patients compared to controls (Materials and methods). A strong positive correlation was found between MVC force and capillary blood lactate changes during the exercise trial in patients with 5qSMA for both BB and TB [r_s (90) = 0.80, P < 0.001, r_s (86) = 0.76, P = 0.002, respectively, Fig. 5C]. We next investigated in the patient group the correlation of capillary blood lactate changes during arm-cycling with of ^{31}P MRS estimates of the fractional intermediate and white myofibre content of their BB and TB muscles. Significant positive correlations were found for both muscles [r_s (112) = 0.61, P = 0.040, r_s (54) = 0.67, P = 0.039, respectively, Fig. 5D]. Last, we explored whether there is any meaningful association between P_i 95% recovery time in white myofibres and the white-to-red myofibre shift in the patient group. For this limited cohort, we lacked statistical power to support any predictive potential at this time but we found for the BB muscle that most patients demonstrated above average (>median score of the control group) on both parameters. (Fig. 5E). We also tested any predictive power of the more facile and commonly used parameter PCr 95% recovery time with respect
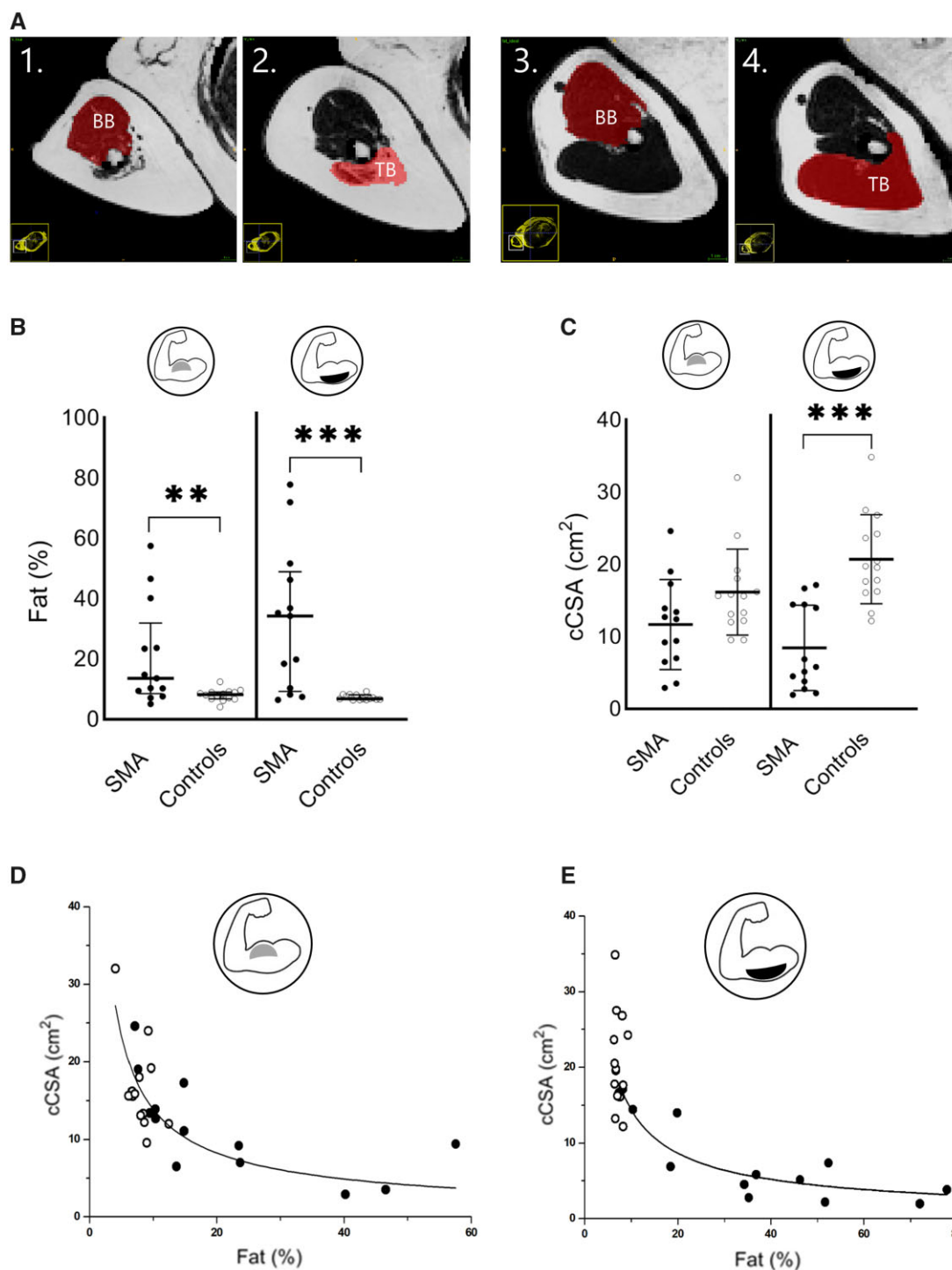
Figure 2 Morphological examination of upper arm musculature of patients with 5qSMA and controls using quantitative MRI. (**A**) MRIs with BB and TB regions of interest in a patient with 5qSMA (1, 2) and a healthy control (3, 4). (**B**) Median, IQR and individual BB ($P = 0.007$) and TB ($P < 0.001$) fat infiltration (%) in 5qSMA and controls. (**C**) Mean, standard deviation and individual BB and TB ($P < 0.001$) contractile cross-sectional area (cCSA) (cm^2) in 5qSMA and controls. (**D** and **E**) Allometric correlation between fat infiltration and cCSA in SMA (open dots) and controls (solid dots); BB: $r = -0.71$, TB: $r = -0.80$. **$P < 0.01$, ***$P < 0.001$.

to white-to-red myofibre shift in the BB muscle but no significant correlation was found (Supplementary Fig. 8).[16]

Discussion

The notion that 5qSMA is a pure motor neuron disease has in recent years been overtaken by the observation that many cell types and tissues are affected by depletion of survival motor neuron protein.[18,53] Specifically, extensive evidence for intrinsic defects of muscle and the neuromuscular junction that are central to 5qSMA pathogenesis has been identified in recent years in both SMA mouse models as well as clinical investigations in patients.[6,10,11,14,17–20,22,54,55] Examples of intrinsic muscular abnormalities in 5qSMA include maladaptive phenotypic remodelling,[8,9]
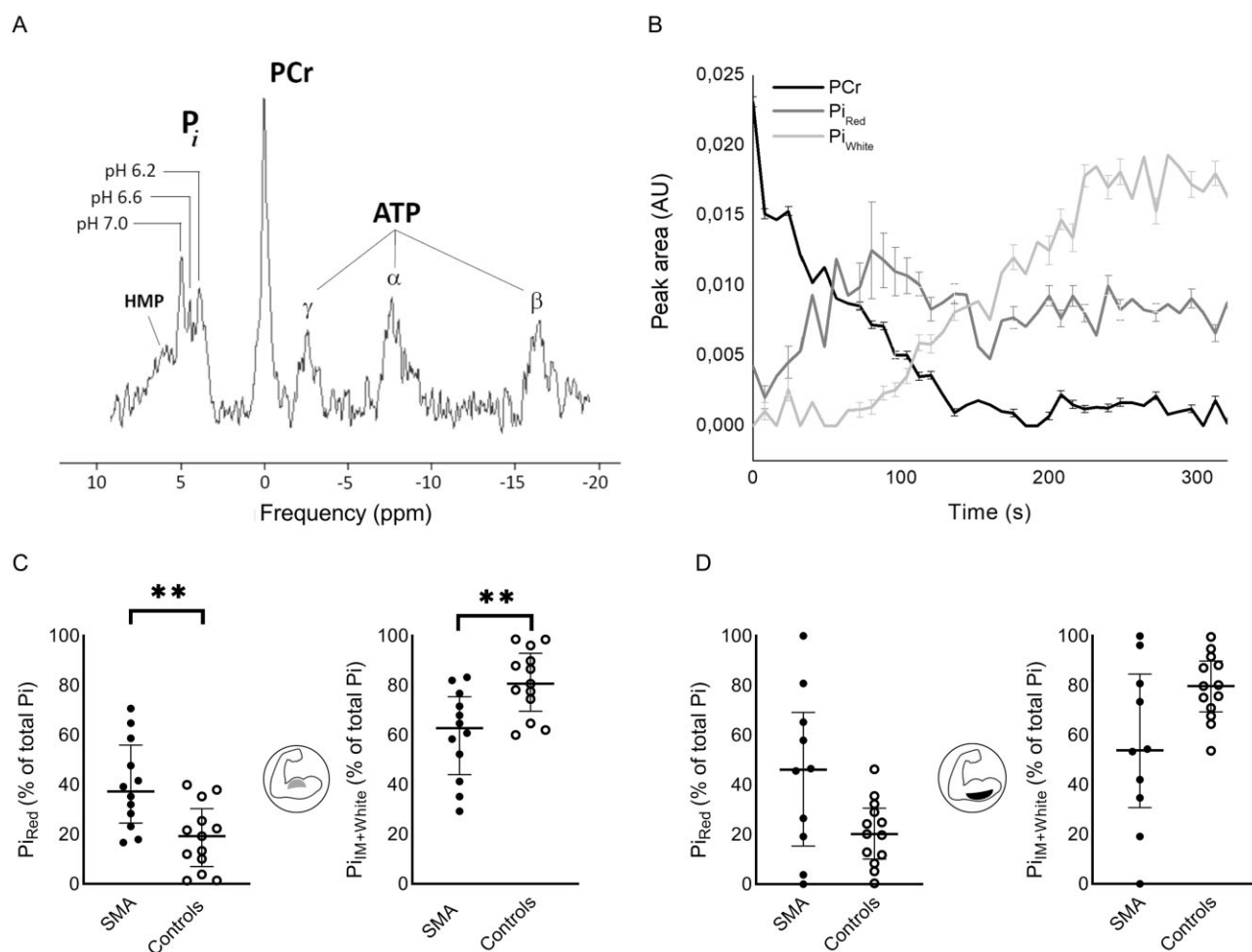
Figure 3 Phenotypic fingerprinting of proximal arm musculature of patients with 5qSMA and healthy controls using dynamic *in vivo* ^{31}P MRS. (A) *In vivo* [31]P magnetic resonance spectrum acquired from BB muscle of a healthy control subject, 60 s after onset of supine arm-cycling exercise at 90 rpm. **(B)** Time course of PCr (black) and Pi in red myofibres operating at pH 7 (dark grey) versus Pi in white fibre operating at pH 6 (light grey) of the BB muscle of an individual patient with 5qSMA performing the arm-cycling at 90 rpm until exhaustion (Supplementary Table 1, Case 10). Error bars represent Cramer–Rao bounds of AMARES fit of ^{31}P magnetic resonance spectra and inform on goodness of fit. The time course of Pi in intermediate (IM) fibres operating at pH 6.6 is omitted for clarity of presentation (Supplementary Fig. 4). **(C and D)** Median, IQR and individual fractional peak area of Pi in red, IM and white myofibres (% of total peak area) in the *in vivo* [31]P magnetic resonance spectrum recorded at exhaustion from BB ($P = 0.004$) and TB ($P = 0.101$) muscles of patients with 5qSMA and controls. **$P < 0.01$.

mitochondrial dysfunction and abnormal sarcomeric calcium handling.[17,19,20] Investigative platforms to further detail these observations in muscle of patients with 5qSMA type 3 and 4 performing a physical task have, however, not yet been available. Here, we exploited quantitative MRI and dynamic *in vivo* ^{31}P MRS methods in combination with a voluntary exercise paradigm to examine muscle morphology and metabolic phenotypic traits in relation to muscle function in adolescent and adult 5qSMA type 3 and 4 *in situ*. Next, we discuss our findings and how they may affect understanding of the clinical presentation of 5qSMA and may guide design and delivery of emergent therapies for this disease.

Understanding muscle weakness in adolescent and adult 5qSMA

Muscle weakness is the main symptom in 5qSMA.[6,7] In our patient cohort, weakness of the proximal arm muscles that were studied here was likewise significant. However, median residual strength of the TB muscle of these individuals was only 15% of controls compared to 55% for the antagonist BB muscle (Fig. 1C). The observation of selective muscle sparing in SMA has previously been reported including in other patients with 5qSMA seen in our centre but remains poorly understood.[6,23–25,27,56,57] Our morphological MRI studies of the upper arm musculature in this cohort offer only a partly explanation of the almost 4-fold difference in decline of strength between the TB and BB muscles in these individuals. Specifically, the residual mean contractile cross-sectional area of the TB muscle in patients was only 40% of controls, whereas there was no significant evidence for atrophy of their BB muscle (Fig. 2C). Closer inspection of these data shows that in a subpopulation of patients atrophy of the TB muscle had progressed even further, to the point that signal degradation in our dynamic *in vivo* ^{31}P MRS recordings from this muscle in some of these individuals prohibited their analysis (Figs 3D and 4D). Regardless, atrophy in and by itself cannot account for the almost 90% decline in strength of the TB muscle in our patients. This is evident when comparing the force per unit contractile cross-sectional area that was 1.4-fold lower in patients (Supplementary Fig. 7). Therefore, altered mechanical properties of the muscle itself must also contribute to this decline.

The comparison of *in vivo* ^{31}P MRS metabolic fingerprints of the BB and TB muscles at exhaustion between patients and controls
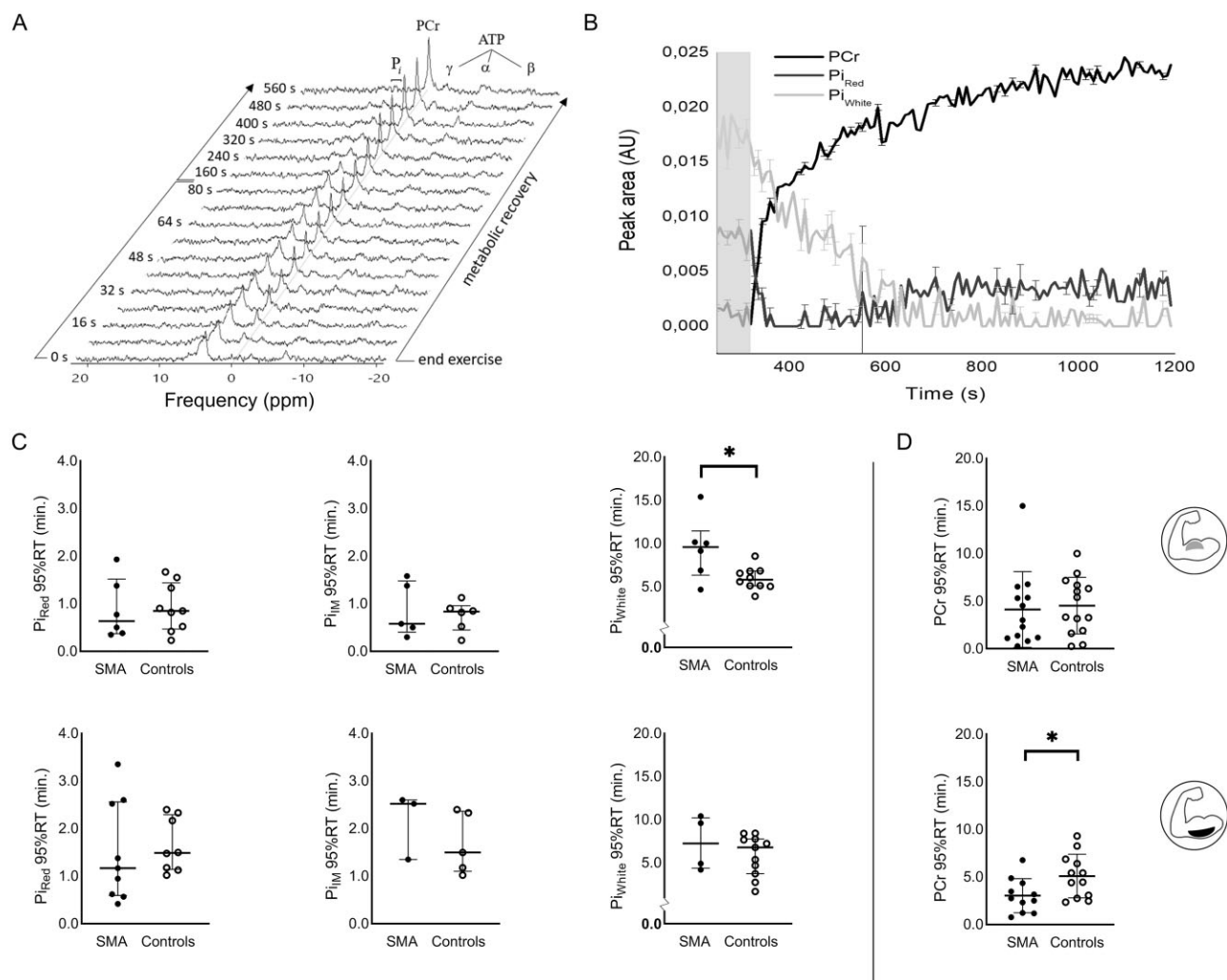
Figure 4 *In vivo* assay of mitochondrial ATP synthetic function in red, intermediate and white myofibres of upper arm muscles of patients with 5qSMA and controls on the basis of dynamic *in vivo* ^{31}P magnetic resonance spectroscopic recordings from BB and TB muscles of patients versus healthy controls post-exercise. (**A**) Stack plot of in vivo ^{31}P nuclear magnetic resonance spectra acquired serially from BB in a patient with 5qSMA starting at the point of exhaustion from preceding arm-cycling exercise and subsequent metabolic recovery. (**B**) Time course of PCr (black) and Pi in red myofibres operating at pH 7 (dark grey) versus Pi in white fibre operating at pH 6 (light grey) of the BB muscle of an individual patient with 5qSMA in final seconds of arm-cycling (shaded area) and subsequent rest (Supplementary Table 1, Case 10). Error bars represent Cramer–Rao bounds of AMARES fit of ^{31}P magnetic resonance spectra and inform on goodness of Lorentzian model fit. The time course of Pi in intermediate (IM) fibres operating at pH 6.6 is omitted for clarity of presentation. (**C**) Median, IQR and individual Pi (red, IM and white) 95% recovery time (RT) (min) in the BB and TB muscle; BB Pi white: $P = 0.031$. (**D**) Mean, standard deviation and individual PCr 95% RT (min) in the BB ($P = 0.764$) and TB ($P = 0.025$) muscle. *$P < 0.05$.

support this conclusion (Fig. 3C and D). In patients, almost 50% of total Pi accumulated in contracting myofibres of the TB muscle at exhaustion originated from red myofibres on the basis of a corresponding myocellular pH of 7, whereas in healthy controls this percentage was only 20% both TB and BB muscles (Fig. 3D). In the latter, the percentage in patients was 40% (Fig. 3C). These results strongly indicate that both the BB and TB muscles in these patients underwent a white-to-red shift with respect to their fibre-type composition. Various laboratories have previously reported similar conclusions on the basis of *in vitro* studies on 5qSMA muscle biopsies from different patients with various types of 5qSMA.[4,8,9,58–62] However, these studies typically examine ~20 μl volumes of muscle causing potential bias. Our in vivo ^{31}P magnetic resonance spectra were obtained from a ~30 000 μl volume of muscle thus mitigating any such concerns.[63] Given the fact that both speed and peak force of red myofibre contractions are substantially lower

than for intermediate and white myofibres,[4] this now provides a mechanistic explanation for the 1.4-fold decline in strength per contractile cross-sectional area of both proximal arm muscles of the patients in this study.

Shifts in fibre-type composition have previously been described in patients with neuromuscular diseases including a red-to-white shift in a fat oxidation defect and are considered to reflect adaptation to the underlying defect.[40,64] On the basis of what has been learned about 5qSMA pathophysiology, it is more likely that a white-to-red shift in myofibre-type composition in this disease is rather the result of a higher vulnerability of fast motor neurons and their associated white musculature to survival motor neuron protein depletion.[23] In this light, we asked whether the latter may be in any way mechanistically linked to the decreased oxidative capacity of white fibres first described in a mouse model of mild SMA by Deguise *et al.*[17] and captured here in patients (Fig. 4C). For
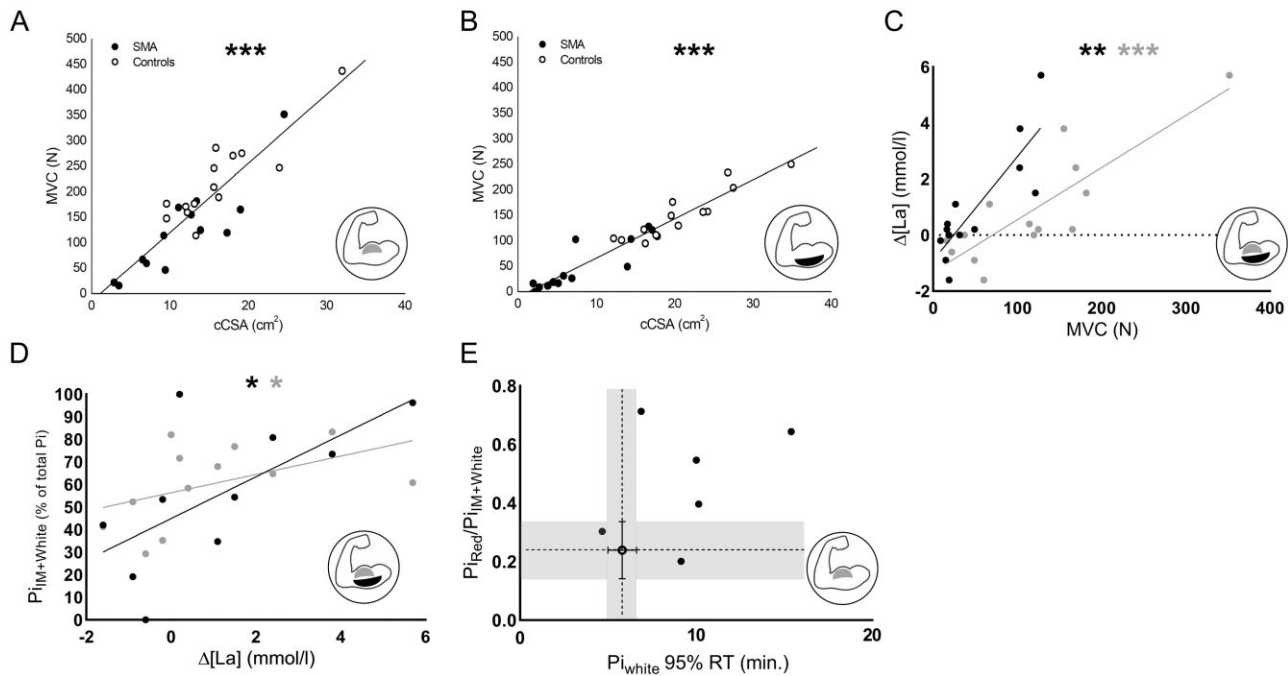
Figure 5 Relationship between muscle ultrastructure, phenotypic traits and function in 5qSMA. (**A** and **B**) Linear correlations between contractile cross-sectional area (cCSA) (cm²) and maximal voluntary contraction (MVC) force (N) of BB and TB; both $P < 0.001$. SMA (solid symbols); controls (open symbols). (**C**) Linear correlations between MVC force (N) and Δ capillary blood lactate (La) (mmol/l) of arm-cycling to exhaustion for BB (grey) and TB (black) muscles of patient with 5qSMA; $P < 0.001$ and $P = 0.002$, respectively. Dashed line indicates Δ[La] = 0. (**D**) Linear correlations between Δ[La] (mmol/l) of arm-cycling to exhaustion and fractional peak area of Pi in intermediate and white myofibres (% of total Pi peak area) in the *in vivo* ³¹P magnetic resonance spectrum recorded at exhaustion from BB (grey) and TB (black) muscles of patients with 5qSMA; $P = 0.040$ and $P = 0.039$, respectively. (**E**) Association of the 95% recovery time (RT) of Pi in white myofibres and ratio of fractional peak area of Pi in red versus intermediate (IM) + white myofibres in the *in vivo* ³¹P magnetic resonance spectrum recorded at exhaustion from BB muscle of patients with 5qSMA (solid symbols). Open symbols: median and IQR of these parameters for BB muscle of healthy controls. Grey area indicates IQR domains. *$P < 0.05$, **$P < 0.01$, ***$P < 0.001$.

this limited cohort, we lacked statistical power to test any correlation but we found that most patients scored above average on both white-to-red shift and an index of mitochondrial oxidative impairment for the BB muscle (Fig. 5E). Future studies in larger patient cohorts will be needed to rigorously test such a correlation.

Understanding muscle fatigability in adolescent and adult 5qSMA

Abnormal muscular fatigability is also a prominent symptom in the clinical presentation of adolescent and adult patients with 5qSMA.[14] In the present study, patients likewise presented with premature fatigue during execution of a physical task, lasting on average less than half the amount of time of their controls during arm-cycling. This was associated with both near maximal perceived fatigue scores as well as near maximal PCr depletion at the end of exercise, similar to controls. While survival motor neuron 2 copy number is generally accepted as the most important modifier for disease severity in 5qSMA,[65] we found no trend between cycling time and survival motor neuron 2 copy number (Supplementary Fig. 10). A previous study from our group in a cohort of 61 patients with 5qSMA type 2, 3 and 4 using a different endurance task likewise found no such association.[14]

In healthy individuals, onset of fatigue during physical work typically reflects failing muscular ATP balance resulting in failing calcium cycling between the myoplasm and the sarcoplasmic reticulum.[15] Based on considerations of ATP-cost per twitch and mitochondrial density,[4] white and intermediate myofibres are at higher risk than red fibres to develop a mismatch between ATP demand and supply during muscular work. Our *in vivo* finding that

post-exercise recovery of Pi in white but not intermediate or red fibres with functional innervation in proximal arm muscle of patients was 40% slower than in healthy controls (Fig. 4C) indicates that mitochondrial ATP synthetic function is compromised specifically in this particular fibre type in 5qSMA type 3 and 4. Houdebine *et al.*[22] came to the same conclusion in a recent study of an SMA mouse model on the basis of biochemical analyses of hindlimb muscles. As a consequence, white fibres of skeletal muscle in this neuromuscular disease are more vulnerable to onset of cellular fatigue mechanisms during physical work.

While this particular outcome of our investigation furthers understanding of abnormal fatigability in 5qSMA, it cannot in and by itself quantitatively explain either our present finding of a 60% reduction in cycling time compared to healthy individuals or previous reports of abnormal fatigability in patients with 5qSMA performing low-intensity endurance tasks.[14,66] First, white myofibres typically make up only 15–20% of total yofiber content in healthy individuals including BB and TB.[4,45,47] In the present study, we found evidence in proximal arm muscle that this percentage may be even lower in 5qSMA (Fig. 3C). Second, post-exercise Pi 95% recovery time in red and intermediate fibres in BB and TB muscles of patients (Fig. 4C) indicated that *in vivo* mitochondrial ATP synthetic capacity in these fibre types is not affected by the disease. This finding also renders any role of muscular capillary defects previously reported in 5qSMA type 1[18,67,68] unlikely in the clinical presentation of 5qSMA type 3 and 4.[69,70] Third, it could be argued that, per unit contractile cross-sectional area, the BB and TB muscles of the patients should have been more, not less resistant than their healthy controls to onset of fatigue mechanisms associated with insufficient ATP supply during arm-cycling. In fact, total

contractile cross-sectional area of the BB muscle did not differ significantly between patients and controls (Fig. 2B). Together, these considerations point to other factors than common myocellular fatigue mechanisms associated with ATP supply–demand imbalance as primary cause of abnormal fatigability in adolescent and adult 5qSMA types 3 and 4.[15]

In light of the accumulated knowledge of 5qSMA pathophysiology,[71] progressive failure of excitation–contraction coupling during task execution at the neuromuscular junction itself is an obvious candidate. Indeed, Deguise *et al.*[17] reported evidence of such neurotransmission impairment in a pioneering mouse model of adult SMA. Using elegant experiments on *ex vivo* nerve–soleus muscle preparations, they found that the force of contractions elicited by nerve versus direct muscle stimulation was up to 25% lower in the former and exhibited a progressive decline not observed in direct muscle stimulation.[17] Notably, the soleus muscle in mice is primarily composed of intermediate (60%) and red (35%) fibres.[50] Their findings indicate that future research to further understanding of the mechanistic basis of abnormal fatigability in 5qSMA should perhaps focus on neuromuscular junction functionality.[55] A further clue pointing towards a primary role of the neuromuscular junction in this matter comes from a recent clinical trial in 5qSMA studying the efficacy of pyridostigmine to enhance neuromuscular signal transmission.[72] Oral administration of this drug reduced fatigability on endurance shuttle tests with 70% but did not affect muscle strength in adolescent and adult patients with 5qSMA type 2–4.[73]

Impact on clinical management and therapy guidance in adolescent and adult 5qSMA

Molecular therapy aimed at rescuing survival motor neuron protein availability in patients with 5qSMA has become available in recent years.[18,74] Both SMN1 gene replacement therapy (i.e. on DNA level) and SMN2-mRNA splicing modification therapies (i.e. on mRNA level) are now available and approved for use in humans.[75] The effect of one of such agents, nusinersen,[76] in children with severe disease (5qSMA type 1) has been promising.[77] However, therapy outcomes in adult patients with comparatively less severe phenotypes (5qSMA types 2 and 3) have been much more variable, with responder rates of 40–50% at best.[78–81] Here, it is important to note that nusinersen delivery in these trials has been done by injection into CSF.[77] As such, its target was exclusively motor neuron populations. However, the notion has been emerging that 5qSMA is not strictly a motor neuron disease and that systemic delivery of these drugs should also be considered.[18] Our present findings do not in and by themselves further this debate, as it remains to be established whether they are the result of a primary muscle defect associated with ubiquitous survival motor neuron depletion or rather secondary to neuromuscular transmission impairment. The latter, however, seems more likely, since any primary muscle defect affecting mitochondrial ATP synthetic capacity may be expected to impact post-exercise Pi recovery across all yofiber types, including red and intermediate myofibres. Our results do indicate that additional use of pharmaceuticals that directly target the muscle and neuromuscular junction, such as pyridostigmine,[73,82] may also benefit these patients, specifically by rescuing excitation–contraction coupling to restore mechanical function and, in its wake, rebuild mitochondrial capacity. In this light, the finding of promising effects of high intensity training in a mild SMA mouse model suggests that such non-pharmaceutical therapy approaches should also be explored in care for adolescent and adult patients with 5qSMA type 3 and 4.[10,22] Specifically, Houdebine *et al.*[22] found that high intensity exercise training over a period of 10 months not only reduced fatigability and protected

the integrity of the neuromuscular junction, but it also reduced intermediate and white motor neuron death and enhanced CSA of large myofibrils.[10] Translating this approach to our present findings in our particular patient cohort, such exercise training could thus potentially improve muscle strength and halt, if not reverse, white-to-red muscle remodelling.[83] Moreover, if the reduced oxidative capacity of white myofibres that we identified in our patients is indeed a consequence of failing neuromuscular transmission aggravated by a state of detraining[84] associated with disuse, then combinatorial treatment of exercise training and pharmaceutical neuromuscular transmission enhancement may reverse also this pathophysiology.[85] The ^{31}P MRS methodology presented here offers various quantitative measures including time to PCr depletion during exercise and 95% recovery time post-exercise that may be used to investigate and tailor the efficacy of such exercise therapy regimens in individual patients. Future studies focusing on development and validation of effective yet safe training programs for patients with 5qSMA are needed.[86]

This study also provides complementary *in vivo* biomarkers and a read-out platform to guide and monitor therapy in 5qSMA and other neuromuscular diseases including sarcopenia.[87] A recent review of the literature on this subject matter concluded that new techniques and biomarkers are needed to improve adult 5qSMA patient stratification, diagnosis and treatment.[81] Current methodologies available to this aim include examination of functional motor unit innervation (i.e. electrophysiological tests),[88–90] morphology (e.g. MRI)[24,27] and functional and physical performance tests (e.g. HFMSE, muscle strength and endurance shuttle tests).[13,91] While each of these methods has its own particular strengths and weaknesses,[81] the *in vivo* ^{31}P MRS methodology presented here may provide added insights such as the nature of the residual functional motor units determined by electrophysiological tests. Moreover, while the latter type of examination is typically not well tolerated, the examination in the present study was very well received and tolerated by all subjects. Our work has identified the *in vivo* ^{31}P MRS phenotypic fingerprint of muscle at the point of exhaustion and post-exercise Pi recovery time in white myofibres as potential novel complementary biomarkers towards this aim. For example, the latter parameter may be particularly useful to investigate which therapy and delivery strategy may prove most effective to restore mitochondrial function in white fibres. With respect to the platform itself, musculoskeletal *in vivo* ^{31}P MRS is a widely used biomedical imaging modality supported by the major MRI vendors.[16] [31]P RF coils and magnetic resonance-compatible cycle-ergometers are likewise commercially available.[16] As such, the arm-cycling magnetic resonance platform used in this study may be assembled without too much difficulty.

Conclusion

This study provides first *in vivo* evidence in patients that degeneration of motor neurons and associated musculature causing atrophy and muscle weakness in 5qSMA type 3 and 4 is aggravated by disproportionate depletion of myofibres that contract fastest and strongest. Our finding of decreased mitochondrial ATP synthetic function selectively in residual white myofibres provides both a possible clue to understanding the apparent vulnerability of this particular fibre type in 5qSMA type 3 and 4 as well as a new biomarker and target for therapy.

Acknowledgements

Funding

Competing interests

W.L.P. is a member of the scientific advisory board of SMA Europe and has served as an *ad hoc* member of the scientific advisory boards of Biogen and Avexis and as a member of a data monitoring committee for Novartis. The other authors report no conflicts of interest.

Supplementary material

Supplementary material is available at *Brain* online.

References

1. Chaytow H, Huang YT, Gillingwater TH, Faller KME. The role of survival motor neuron protein (SMN) in protein homeostasis. *Cell Mol Life Sci*. 2018;75(21):3877–3894.

2. Lefebvre S, Bürglen L, Reboullet S, et al. Identification and characterization of a spinal muscular atrophy-determining gene. *Cell*. 1995;80(1):155–165.

3. Boyer JG, Bowerman M, Kothary R. The many faces of SMN: Deciphering the function critical to spinal muscular atrophy pathogenesis. *Future Neurol*. 2010;5(6):873–890.

4. Schiaffino S, Reggiani C. Fiber types in mammalian skeletal muscles. *Physiol Rev*. 2011;91(4):1447–1531.

5. Glancy B, Balaban RS. Protein composition and function of red and white skeletal muscle mitochondria. *Am J Physiol – Cell Physiol*. 2011;300(6):1280–1290.

6. Wadman RI, Wijngaarde CA, Stam M, et al. Muscle strength and motor function throughout life in a cross-sectional cohort of 180 patients with SMA types 1c-4. *Eur J Neurol*. 2018;25(3):512–518.

7. Munsat TL, Davies KE. International SMA Consortium Meeting (26-28 June 1992, Bonn, Germany). *Neuromuscul Disord*. 1992;2(5-6):423–428.

8. Anderson JR. Atlas of skeletal muscle pathology. In: Gresham GA, ed. *Atlas of skeletal muscle pathology*, 9th ed. MTP Press Limited; 1985: 46–52.

9. Johnson MA, Kucukyalcin DK. Patterns of abnormal histochemical fibre type differentiation in human muscle biopsies. *J Neurol Sci*. 1978;37(3):159–178.

10. Chali F, Desseille C, Houdebine L, et al. Long-term exercise-specific neuroprotection in spinal muscular atrophy-like mice. *J Physiol*. 2016;594(7):1931–1952.

11. Stam M, Wadman RI, Bartels B, et al. A continuous repetitive task to detect fatigability in spinal muscular atrophy. *Orphanet J Rare Dis*. 2018;13(1):1–7.

12. Bartels B, Habets LE, Stam M, et al. Assessment of fatigability in patients with spinal muscular atrophy: Development and content validity of a set of endurance tests. *BMC Neurol*. 2019;19(1):1–10.

13. Bartels B, Groot JD, Habets LE, et al. Fatigability in spinal muscular atrophy: Validity and reliability of endurance shuttle tests. *Orphanet J Rare Dis*. 2020;15(1):1–9.

14. Bartels B, de Groot JF, Habets LE, et al. Correlates of fatigability in patients with spinal muscular atrophy. *Neurology*. 2020;96(6):e845–e852.

15. Cheng AJ, Place N, Westerblad H. Molecular basis for exercise-induced fatigue: The importance of strictly controlled cellular Ca^{2+} handling. *Cold Spring Harb Perspect Med*. 2018;8(2):a029710.

16. Meyerspeer M, Boesch C, Cameron D, et al. 31P magnetic resonance spectroscopy in skeletal muscle: Experts' consensus recommendations. *NMR Biomed*. 2020;34(5):e4246.

17. Deguise MO, De Repentigny Y, Tierney A, et al. Motor transmission defects with sex differences in a new mouse model of mild spinal muscular atrophy. *EbioMedicine*. 2020;55:102750.

18. Yeo CJJ, Darras BT. Overturning the paradigm of spinal muscular atrophy as just a motor neuron disease. *Pediatr Neurol*. 2020;109:12–19.

19. Miller N, Shi H, Zelikovich A, Ma Y-C. Motor neuron mitochondrial dysfunction in spinal muscular atrophy. *Hum Mol Genet*. 2016;25(16):3395–3406.

20. Ripolone M, Ronchi D, Violano R, et al. Impaired muscle mitochondrial biogenesis and myogenesis in spinal muscular atrophy. *JAMA Neurol*. 2015;72(6):666–675.

21. Shababi M, Lorson CL, Rudnik-Schöneborn SS. Spinal muscular atrophy: A motor neuron disorder or a multi-organ disease? *J Anat*. 2014;224(1):15–28.

22. Houdebine L, D'Amico D, Bastin J, et al. Low-intensity running and high-intensity swimming exercises differentially improve energy metabolism in mice with mild spinal muscular atrophy. *Front Physiol*. 2019;10:1258.

23. Boyd PJ, Tu WY, Shorrock HK, et al. Bioenergetic status modulates motor neuron vulnerability and pathogenesis in a zebrafish model of spinal muscular atrophy. *PloS Genet*. 2017;13(4):e1006744.

24. Otto LAM, van der Pol WL, Schlaffke L, et al. Quantitative MRI of skeletal muscle in a cross-sectional cohort of patients with spinal muscular atrophy types 2 and 3. *NMR Biomed*. 2020;33(10):e4357.

25. Chabanon A, Seferian AM, Daron A, et al.; The NatHis-SMA study group. Prospective and longitudinal natural history study of patients with Type 2 and 3 spinal muscular atrophy: Baseline data NatHis-SMA study. *PloS ONE*. 2018;13(7):e0201004.

26. Bonati U, Holiga Š, Hellbach N, et al. Longitudinal characterization of biomarkers for spinal muscular atrophy. *Ann Clin Transl Neurol*. 2017;4(5):292–304.

27. Brogna C, Cristiano L, Verdolotti T, et al. MRI patterns of muscle involvement in type 2 and 3 spinal muscular atrophy patients. *J Neurol*. 2020;267(4):898–912.

28. Mizuno M, Justesen LO, Bedolla J, Friedman DB, Secher NH, Quistorff B. Partial curarization abolishes splitting of the inorganic phosphate peak in 31P-NMR spectroscopy during intense forearm exercise in man. *Acta Physiol Scand*. 1990;139(4):611–612.

29. Mizuno M, Horn A, Secher NH, Quistorff B. Exercise-induced 31P-NMR metabolic response of human wrist flexor muscles during partial neuromuscular blockade. *Am J Physiol – Regul Integr Comp Physiol*. 1994;267(2):R408–R414.

30. D'Amico A, Mercuri E, Tiziano FD, Bertini E. Spinal muscular atrophy. *Orphanet J Rare Dis*. 2011;6:71.

31. Beenakker EAC, Van der Hoeven JH, Fock JM, Maurits NM. Reference values of maximum isometric muscle force obtained in 270 children aged 4-16 years by hand-held dynamometry. *Neuromuscul Disord*. 2001;11(5):441–446.

32. Juel C. Lactate/proton co-transport in skeletal muscle: Regulation and importance for pH homeostasis. *Acta Physiol Scand*. 1996;156(3):369–374.

33. Juel C. Lactate-proton cotransport in skeletal muscle. *Physiol Rev*. 1997;77(2):321–358.

34. Vegter RJ, Brink S V D. Mouton, L Sibeijn-Kuiper, A Woude, L Jeneson, J. Magnetic resonance-compatible arm-crank ergometry: A new platform linking whole-body calorimetry to upper-extremity biomechanics and arm muscle metabolism. *Front Neurol*. 2021;12:1–13.

35. Jeneson JAL, Schmitz JPJ, Hilbers PAJ, Nicolay K. An MR-compatible bicycle ergometer for in-magnet whole-body human exercise testing. *Magn Reson Med*. 2010;63(1):257–261.

36. Henneman E, Clamann HP, Gillies JD, Skinner RD. Rank order of motoneurons within a pool: Law of combination. *J Neurophysiol*. 1974;37(6):1338–1349.

37. Schlaffke L, Rehmann R, Rohm M. Multi-center evaluation of stability and reproducibility of quantitative MRI measures in healthy calf muscles. *NMR Biomed*. 2019;32(9):1–14.

38. Yushkevich PA, Piven J, Hazlett HC, et al. User-guided 3D active contour segmentation of anatomical structures: Significantly improved efficiency and reliability. *Neuroimage*. 2006;31(3):1116–1128.

39. Rzanny R, Stutzig N, Hiepe P, Gussew A, Thorhauer HA, Reichenbach JR. The reproducibility of different metabolic markers for muscle fiber type distributions investigated by functional 31P-MRS during dynamic exercise. *Z Med Phys*. 2016;26(4):323–338.

40. Diekman EF, Visser G, Schmitz JPJ, et al. Altered energetics of exercise explain risk of rhabdomyolysis in very long-chain acyl-CoA dehydrogenase deficiency. *PloS ONE*. 2016;11(2):e0147818.

41. Werkman M, Jeneson J, Helders P, et al. Exercise oxidative skeletal muscle metabolism in adolescents with cystic fibrosis. *Exp Physiol*. 2016;101(3):421–435.

42. Vandenborne K, McCully K, Kakihira H, et al. Metabolic heterogeneity in human calf muscle during maximal exercise. *Proc Natl Acad Sci USA*. 1991;88(13):5714–5718.

43. Vegter RJK, Hartog J, De Groot S, et al. Early motor learning changes in upper-limb dynamics and shoulder complex loading during handrim wheelchair propulsion. *J Neuroeng Rehabil*. 2015;12(1):1–14.

44. Schmitz JPJ, van Riel NAW, Nicolay K, Hilbers PAJ, Jeneson JAL. Silencing of glycolysis in muscle: Experimental observation and numerical analysis. *Exp Physiol*. 2010;95(2):380–397.

45. Johnson MA, Polgar J, Weightman D, Appleton D. Data on the distribution of fibre types in thirty-six human muscles. *J Neurol Sci*. 1973;18(1):111–129.

46. Nygaard E, Houston M, Suzuki Y, Jørgensen K, Saltin B. Morphology of the brachial biceps muscle and elbow flexion in man. *Acta Physiol Scand*. 1983;117(2):287–292.

47. Klitgaard H, Mantoni M, Schiaffino S, et al. Function, morphology and protein expression of ageing skeletal muscle: A cross-sectional study of elderly men with different training backgrounds. *Acta Physiol Scand*. 1990;140(1):41–45.

48. Meyer RA. A linear model of muscle respiration explains monoexponential phosphocreatine changes. *Am J Physiol – Cell Physiol*. 1988;254(4 Pt 1):C548–C553.

49. Glancy B, Hsu L-Y, Dao L, et al. In Vivo microscopy reveals extensive embedding of capillaries within the sarcolemma of skeletal muscle fibers. *Microcirculation*. 2014;21(2):131–147.

50. Ciapaite J, van den Berg SA, Houten SM, Nicolay K, Willems van Dijk K, Jeneson JA. Fiber-type-specific sensitivities and phenotypic adaptations to dietary fat overload differentially impact fast- versus slow-twitch muscle contractile function in C57BL/6J mice. *J Nutr Biochem*. 2015;26(2):155–164.

51. Kemp G, Thompson CH, Barnes PRJ, Radda G. Comparisons of ATP turnover in human muscle during ischemic and aerobic exercise using 31P magnetic resonance spectroscopy. *Magn Reson Med*. 1994;31(3):248–258.

52. Bendahan D, Confort-Gouny S, Kozak-Reiss G, Cozzone PJ. Heterogeneity of metabolic response to muscular exercise in humans. New criteria of invariance defined by in vivo phosphorus-31 NMR spectroscopy. *FEBS Lett*. 1990;272(1-2):155–158.

53. Hamilton G, Gillingwater TH. Spinal muscular atrophy: Going beyond the motor neuron. *Trends Mol Med*. 2013;19(1):40–50.

54. Khayrullina G, Moritz KE, Schooley JF, et al. SMN-deficiency disrupts SERCA2 expression and intracellular Ca^{2+} signaling in cardiomyocytes from SMA mice and patient-derived iPSCs. *Skelet Muscle*. 2020;10(1):16.

55. Wadman RI, Vrancken AFJE, van den Berg LH, van der Pol WL. Van den Berg LH, Van der Pol WL. Dysfunction of the neuromuscular junction in patients with spinal muscular atrophy type 2 and 3. *Neurology*. 2012;79(20):2050–2055.

56. Piepers S, van den Berg LH, Brugman F, et al. A natural history study of late onset spinal muscular atrophy types 3b and 4. *J Neurol*. 2008;255(9):1400–1404.

57. Deymeer F, Serdaroglu P, Parman Y, Poda M. Natural history of SMA IIIb: Muscle strength decreases in a predictable sequence and magnitude. *Neurology*. 2008;71(9):644- 649.

58. Dubowitz V. Pathology of experimentally re-innervated skeletal muscle. *J Neurol Neurosurg Psychiatry*. 1967;30(2):99–110.

59. Dubowitz V. Enzyme histochemistry of skeletal muscle. 3. Neurogenic muscular atrophies. *J Neurol Neurosurg Psychiatry*. 1966;29(1):23–28.

60. Hausmanowa-Petrusewicz I, Askanas W, Badurska B, et al. Infantile and juvenile spinal muscular atrophy. *J Neurol Sci*. 1968;6(2):269–287.

61. Mastaglia FL, Walton JN. Histological and histochemical changes in skeletal muscle from cases of chronic juvenile and early adult spinal muscular atrophy (the Kugelberg-Welander syndrome). *J Neurol Sci*. 1971;12(1):15–44.

62. Scott W, Stevens J, Binder–Macleod SA. Human skeletal muscle fiber type classifications. *Phys Ther*. 2001;81(11):1810–1816.

63. Jeneson JAL, van Dobbenburgh JO, van Echteld CJA, et al. Experimental design of 31P MRS assessment of human forearm muscle function: Restrictions imposed by functional anatomy. *Magn Reson Med*. 1993;30(5):634–640.

64. Imoto C, Nonaka I. The significance of type 1 fiber atrophy (hypotrophy) in childhood neuromuscular disorders. *Brain Dev*. 2001;23(5):298–302.

65. Wadman RI, Jansen MD, Stam M, et al. Intragenic and structural variation in the SMN locus and clinical variability in spinal muscular atrophy. *Brain Commun*. 2020;2(2):fcaa075.

66. Montes J, Dunaway S, Garber CE, Chiriboga CA, De Vivo DC, Rao AK. Leg muscle function and fatigue during walking in spinal muscular atrophy type 3. *Muscle Nerve*. 2014;50(1):34–39.

67. Zhou H, Ying H, Scoto M, Brogan P, Parson S, Muntoni F. Microvascular abnormality in spinal muscular atrophy and its response to antisense oligonucleotide therapy. *Neuromuscul Disord*. 2015;25(2015):S193.

68. Somers E, Lees RD, Hoban K, et al. Vascular defects and spinal cord hypoxia in spinal muscular atrophy. *Ann Neurol*. 2016;79(2):217–230.

69. Van Brussel M, van Oorschot JWM, Schmitz JPJ, et al. Muscle metabolic responses during dynamic in-magnet exercise testing: A pilot study in children with an idiopathic inflammatory myopathy. *Acad Radiol*. 2015;22(11):1443–1448.

70. Cea G, Bendahan D, Manners D et al. Reduced oxidative phosphorylation and proton efflux suggest reduced capillary blood supply in skeletal muscle of patients with dermatomyositis and polymyositis: A quantitative 31 P-magnetic resonance spectroscopy and MRI study. *Brain*. 2002;125(Pt 7):1635–1645.

71. Faravelli I, Nizzardo M, Comi GP, Corti S. Spinal muscular atrophy—recent therapeutic advances for an old challenge. *Nat Rev Neurol*. 2015;11(6):351–359.

72. Stam M, Wadman RI, Wijngaarde CA, et al. Protocol for a phase II, monocentre, double-blind, placebo-controlled, cross-over trial to assess efficacy of pyridostigmine in patients with spinal muscular atrophy types 2-4 (SPACE trial). *BMJ Open*. 2018;8(7): e019932.

73. Stam M, Wijngaarde C, Bartels B et al. Space trial. A phase 2, monocenter, double-blind, placebo-controlled, cross-over trial to assess efficacy of pyridostigmine in patients with spinal muscular atrophy types 2,3 and 4. In: Cure SMA, June 30, 2019; 2019.

74. Bowerman M, Becker CG, Yáñez-Muñoz RJ, et al.; UK SMA Research Consortium. Therapeutic strategies for spinal muscular atrophy: SMN and beyond. *DMM Dis Model Mech*. 2017;10(8): 943–954.

75. Wirth B, Karakaya M, Kye MJ, Mendoza-Ferreira N. Twenty-five years of spinal muscular atrophy research: From phenotype to genotype to therapy, and what comes next. *Annu Rev Genomics Hum Genet*. 2020;21:231–261.

76. Passini M. A, Bu J, Richards AM, et al. Antisense oligonucleotides delivered to the mouse CNS ameliorate symptoms of severe spinal muscular atrophy. *Sci Transl Med*. 2011;3(72):72ra18.

77. Finkel RS, Mercuri E, Darras BT, et al. Nusinersen versus sham control in infantile-onset spinal muscular atrophy. *N Engl J Med*. 2017;377(18):1723–1732.

78. Walter MC, Wenninger S, Thiele S, et al. Safety and treatment effects of nusinersen in longstanding adult 5q-SMA type 3 – a prospective observational study. *J Neuromuscul Dis*. 2019;6(4): 453–465.

79. Hagenacker T, Wurster CD, Günther R, et al. Nusinersen in adults with 5q spinal muscular atrophy: a non-interventional, multicentre, observational cohort study. *Lancet Neurol*. 2020; 19(4):317–325.

80. Jochmann E, Steinbach R, Jochmann T, et al. Experiences from treating seven adult 5q spinal muscular atrophy patients with Nusinersen. *Ther Adv Neurol Disord*. 2020;13:1756286420907803.

81. Smeriglio P, Langard P, Querin G, Biferi MG. The identification of novel biomarkers is required to improve adult SMA patient stratification, diagnosis and treatment. *J Pers Med*. 2020;10(3):75.

82. Riker WF, Wescoe WC. The direct action of prostigmine on skeletal muscle; its relationship to the choline esters. *J Pharmacol Exp Ther*. 1946;88(1):58–66.

83. Fitts RH. Cellular mechanisms of skeletal muscle fatigue. *Pysiological Rev*. 1994;74(1):49–81.

84. Wibom R, Hultman E, Johansson M, Matherei K, Constantin-Teodosiu D, Schantz PG. Adaptation of mitochondrial ATP production in human skeletal muscle to endurance training and detraining. *J Appl Physiol*. 1992;73(5):2004–2010.

85. Westerblad H, Bruton JD, Katz A. Skeletal muscle: Energy metabolism, fiber types, fatigue and adaptability. *Exp Cell Res*. 2010; 316(18):3093–3099.

86. Bartels B, Montes J, Van Der Pol WL, De Groot JF. Physical exercise training for type 3 spinal muscular atrophy. *Cochrane Database Syst Rev*. 2019;3(3):CD012120.

87. Larsson L, Degens H, Li M, et al. Sarcopenia: Aging-related loss of muscle mass and function. *Physiol Rev*. 2019;99(1):427–511.

88. Sleutjes BTHM, Wijngaarde CA, Wadman RI, et al. Assessment of motor unit loss in patients with spinal muscular atrophy. *Clin Neurophysiol*. 2020;131(6):1280–1286.

89. Querin G, Lenglet T, Debs R, et al. The motor unit number index (MUNIX) profile of patients with adult spinal muscular atrophy. *Clin Neurophysiol*. 2018;129(11):2333–2340.

90. Verma S, Forte J, Ritchey M, Shah D. Motor unit number index in children with later-onset spinal muscular atrophy. *Muscle and Nerve*. 2020;62(5):633–637.

91. Glanzman AM, O'Hagen J, McDermott M, et al. Validation of the expanded hammersmith functional motor scale in spinal muscular atrophy type II and III. *J Child Neurol*. 2011;26(12): 1499–1507.